Synthesis and photocatalytic properties of Co- and Cu-doped $Bi_2Sn_2O_7$

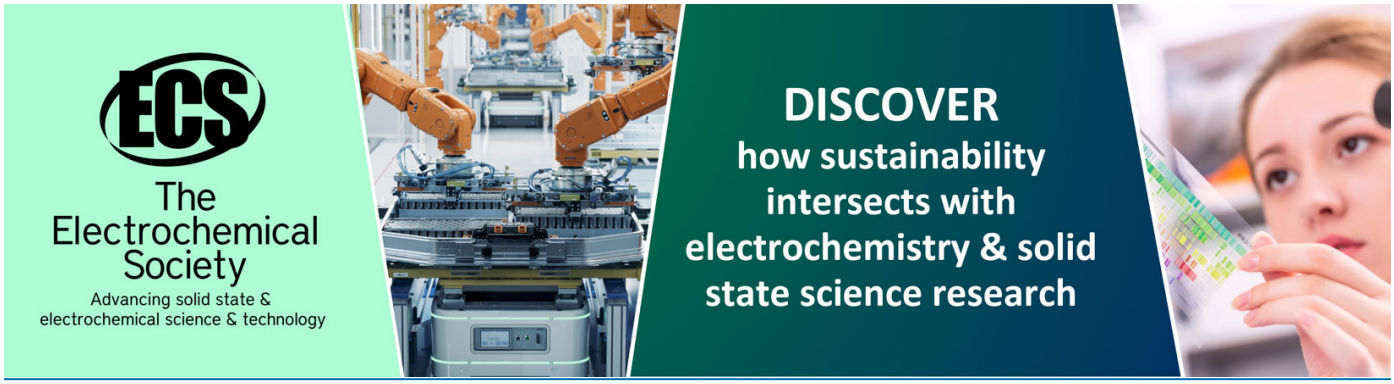

Synthesis and photocatalytic properties of Co- and Cu-doped $Bi_2Sn_2O_7$

Jing Zhuang[1, 2], Chaohao Hu[1, 2, 3], Binqing Zhu[1, 2], Yan Zhong[1, 2], and Huaiying Zhou[1, 2]

[1] Guangxi Key Laboratory of Information Materials, Guilin University of Electronic Technology, Guilin 541004, P.R. China
[2] School of Materials Science and Engineering, Guilin University of Electronic Technology, Guilin 541004, P.R. China

E-mail: chaohao.hu@guet.edu.cn

Abstract. $Bi_2Sn_2O_7$ photocatalysts doped by Co and Cu ions were successfully synthesized by using the hydrothermal process and impregnation method. The products were characterized using X-ray diffraction analysis (XRD), Field emission scanning electron microscopy (FESEM), Energy dispersive X-ray detector (EDS), infrared spectroscopy (IR), the photoluminescence (PL) spectra and UV-visible diffuse reflectance spectroscopy (DRS). The photocatalytic properties were further evaluated by degrading rhodamine B (RhB) as a model pollution under visible-light irradiation. The results indicated that Co- and Cu-doped $Bi_2Sn_2O_7$ photocatalysts have a cubic pyrochlore phase with the hybrid metals. The metal-loaded photocatalysts show the enhanced photocatalytic efficiency for degradation of RhB under visible-light (λ> 420 nm). The mechanism of improved photocatalytic activity is also discussed in detail.

1. Introduction

Environmental pollution has become a serious problem in the past few decades with the rapid development of industrial technology and economy. Among a great number of the advanced oxidation processes, semiconductor photocatalytic oxidation is regarded as a green technology to decompose the soluble dyes in wastewater and eliminate toxic chemicals in the environment [1-6]. So far TiO_2 is the most studied semiconductor photocatalyst due to the outstanding oxidative power, low cost, non-toxicity and chemical stability. However, TiO_2 is only active under ultraviolet (UV) light irradiation because of its large band gap (about 3.2 eV for anatase). It is important to develop new photocatalysts responsive to visible-light irradiation with the enhanced photocatalytic activity in order to make full use of solar energy [7-9].

Currently, $Bi_2Sn_2O_7$ has received considerable attention because of its wide application in catalysis and gas sensors in recent years [10,11]. $Bi_2Sn_2O_7$ belongs to the pyrochlore family with the general formula $A_2B_2O_7$, where A-cations are eight coordinated and B-cations are six coordinated [12]. As shown in Figure 1, the crystal structure of $Bi_2Sn_2O_7$ is constructed of SnO_6 octahedra and BiO_8 dodecahedra in which SnO_6 and BiO_8 connect to each other by sharing vertexes and edges, respectively. Recently, Tian et al. [13] have investigated the photooxidation of As(III) under visible-light irradiation of $Bi_2Sn_2O_7$. Wu et al. [14] have synthesized nano-$Bi_2Sn_2O_7$ by a hydrothermal method and studied its photocatalytic activity in the degradation of methyl orange. However, the photocatalytic activity of individual $Bi_2Sn_2O_7$ is relatively low. The photocatalytic performance of $Bi_2Sn_2O_7$ should be further

improved for practical use. Recently, Liu et al. [15] have synthesized $Bi_2Sn_2O_7$/reduced graphene oxide nanocomposite for efficient photocatalytic degradation of organic contaminants. Mohamed et al. [16] have prepared Pd-doped-Bi_2O_3/$Bi_2Sn_2O_7$ hybrid nanocomposites for photocatalytic fluorene oxidation.

In this study, metal-doped catalysts Cu-$Bi_2Sn_2O_7$ and Co-$Bi_2Sn_2O_7$ were successfully synthesized by using the hydrothermal process and wet-impregnation method. The crystal structure, morphologies, particle sizes and optical properties were investigated by various techniques. The photocatalytic activities of the composite samples were evaluated by the photocatalytic discoloration of rhodamine B (RhB) under visible light irradiation.

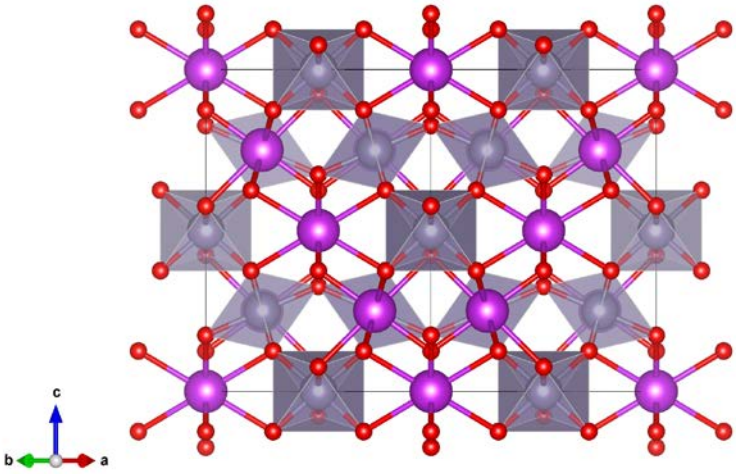

Figure 1. Crystal structure of $Bi_2Sn_2O_7$. The purple, gray, and red spheres are for Bi, Sn, and O atoms, respectively.

2. Experimental procedures

2.1. Synthesis

All chemicals were reagent grade and used without further purification. The cubic pyrochlore $Bi_2Sn_2O_7$ powders were synthesized in a typical hydrothermal processing. First, 0.01 mol $Bi(NO_3)_3{\cdot}5H_2O$ and 0.01 mol $SnCl_4{\cdot}5H_2O$ were dissolved in 30 ml deionized water and stirred for 20 min at room temperature. Then the pH value of the mixture was adjusted to 12 by using 4 mol/L NaOH. The mixed solution was stirred continuously at room temperature for 30 min, then transferred into Teflon-lined autoclave (100 mL capacity, 80% full) and kept at 200 ℃ for 16 h in an oven. After the reaction, The as-prepared products were collected after washing with deionized water and anhydrous ethanol several times, respectively. At last, the products were dried at 60℃ for 12 h in an oven.

M-$Bi_2Sn_2O_7$ (M = Cu, Co) catalysts were prepared by the impregnation method from the aqueous solutions of $Cu(NO_3)_2$ and $Co(NO_3)_2$. The mass ratio of $Cu(NO_3)_2$ and $Co(NO_3)_2$ to $Bi_2Sn_2O_7$ is 1:20. The as-prepared $Bi_2Sn_2O_7$ powder was added to anhydrous ethanol (10 mL) containing an certain amount of $Cu(NO_3)_2$ and $Co(NO_3)_2$ in a ceramic dish. The suspension was stirred using a glass rod during the irradiation of infrared light until the evaporation of anhydrous ethanol. Finally, the dried powders were calcined in alumina crucible at 600℃ for 4 h.

2.2. Characterization

Crystal structures of $Bi_2Sn_2O_7$ and M-$Bi_2Sn_2O_7$ catalysts were characterized by powder X-ray diffraction (XRD) (Bruker D8-2-Advanced XRD, Germany) using Cu Kα radiation (λ = 0.1541 nm) from 10º to 80º, with a scan speed of 5º min^{-1}. The morphologies and microstructures of the as-prepared catalysts were observed using the field emission scanning electron microscopy (FESEM, Quanta 450 FEG, USA). The chemical composition of the samples was examined using the energy dispersive X-ray detector (EDS) (Thermo Noran VANTAG-ESI, USA).The photoluminescence (PL) spectra were measured using a fluorescence spectrophotometer at room temperature (Varian, USA) with an excitation wavelength of 380 nm. Fourier transform infrared (FT-IR) spectra were recorded on FTIR spectrometer (Thermo Fisher Nicolet 6700) using the standard KBr disk method. The UV-vis absorption spectra of the photocatalysts were obtained by a UV-vis spectrometer (Puxi TU-1901, China) in the range of 200-700 nm, using $BaSO_4$ as the reference sample.

2.3. Photocatalytic activity test

The photocatalytic efficiency of all of the prepared samples was evaluated by degrading RhB under visible-light irradiation at room temperature. The 0.10 g powder of photocatalyst was immersed in a quartz beaker containing 100 mL RhB solution with a concentration of 5 mg/L. In order to ensure the adsorption/desorption equilibrium between RhB and photocatalyst, the suspension was stirred in the dark for 30 min. Xeon arc lamp with 300 W through UV cut-off filters placed at about 10 cm from the reactor completely removes any radiation below 420 nm and offer visible light source. After the photocatalytic reactions, 5 mL of suspensions was taken out at given time intervals. At last, a centrifuge was used to remove the powder and the supernatant was taken for analysis. The absorbance of centrifugal solution was determined at 553 nm by UV-vis spectrophotometer.

3. Results and Discussion

3.1. Structural and morphological characterization

The measured XRD shown in Figure 2 indicates that the diffraction peaks of all of the samples were indexed to the standard card of pure cubic phase of $Bi_2Sn_2O_7$ (JCPDS No. 87-0284). The characteristic peaks of the three samples at 2θ = 28.8°, 33.3°, 47.9°, 56.9° are obvious and no other impurity peaks can be observed, indicating high purity of the final products. The doped Co and Cu do not change the crystal structure of $Bi_2Sn_2O_7$, implying that Cu and Co are loaded onto the surface of the $Bi_2Sn_2O_7$. According to Debye-Scherrer equation [17] with the shape factor K = 0.89, the calculated crystallite size of three samples is about 21.1 nm based on the main diffraction peak (222). In addition, the diffraction peaks of Co and Cu cannot be observed probably due to the low amount of the hybrid metals.

The IR spectra of the pure $Bi_2Sn_2O_7$ and M-$Bi_2Sn_2O_7$ samples are shown in Figure 3. The bands centered at about 3420 and 1640 cm^{-1} are assigned to O-H stretching and bending modes of water, respectively [18]. The band at about 621 cm^{-1} can be assigned to the B-O stretching vibration in the BO_6 octahedron, which is comparable with the A-O stretching vibration of pyrochlore $A_2B_2O_7$ centered at about 517 cm^{-1} reported by Subramanian and co-authors [19]. The weak bands at about 422 cm^{-1} are ascribed to the Bi-O-Bi bending vibrations, which is similar to the previous experimental results presented by Xu and co-authors [20]. Compared with the pure $Bi_2Sn_2O_7$ sample, the peak at about 621 cm^{-1} for M-$Bi_2Sn_2O_7$ is sharper and has a little blue shift.

Figure 4 shows the SEM images of pure and metal doped $Bi_2Sn_2O_7$. Our results indicate that the size of particles mainly ranges from 2 to 4 μm. It can be seen that the micro morphology of pure $Bi_2Sn_2O_7$ catalysts are composed of layered pompons and particles. The pompons in M-$Bi_2Sn_2O_7$ are packed closer to each other, which may be caused by a heterojunction between the metal particles and $Bi_2Sn_2O_7$ after loading the metals. The morphology and microstructure of Cu-$Bi_2Sn_2O_7$ is rose-shaped and that in Co-$Bi_2Sn_2O_7$ is consisted of more regular layered pompon. The EDS analysis was carried out in order to determine the elemental composition of M-$Bi_2Sn_2O_7$. Bi, Sn, O, Co and Cu elements can be found from the EDS energy spectra as presented in Figure 5(a-b).

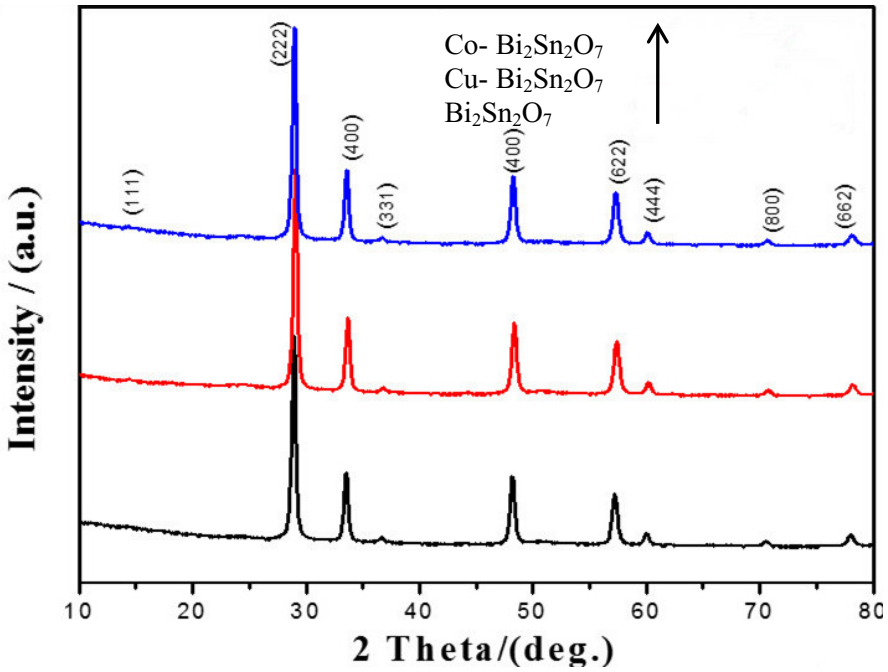

Figure 2. XRD patterns of pure $Bi_2Sn_2O_7$ and M-$Bi_2Sn_2O_7$

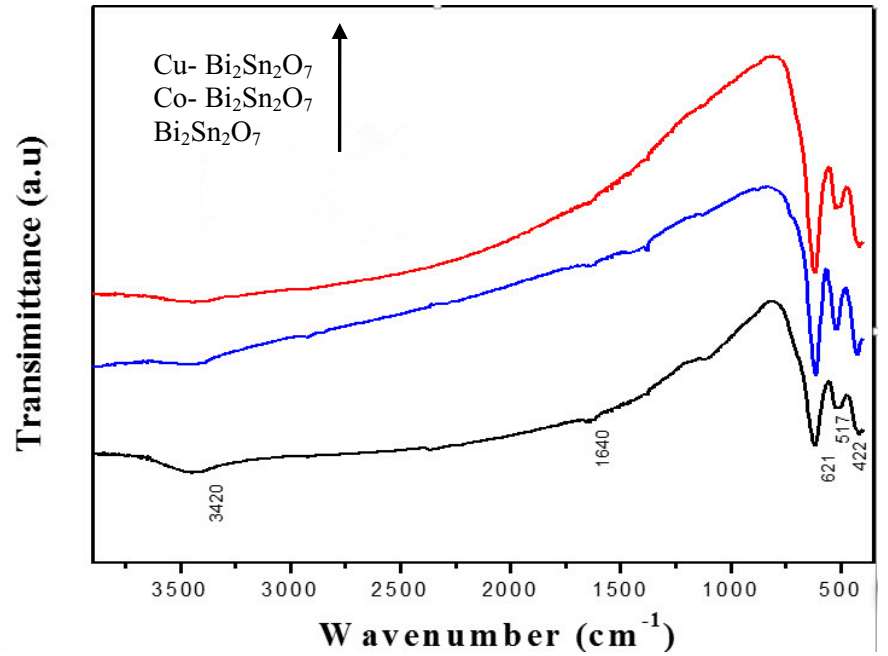

Figure 3. IR spectra of the as-prepared pure $Bi_2Sn_2O_7$ and M-$Bi_2Sn_2O_7$ powders

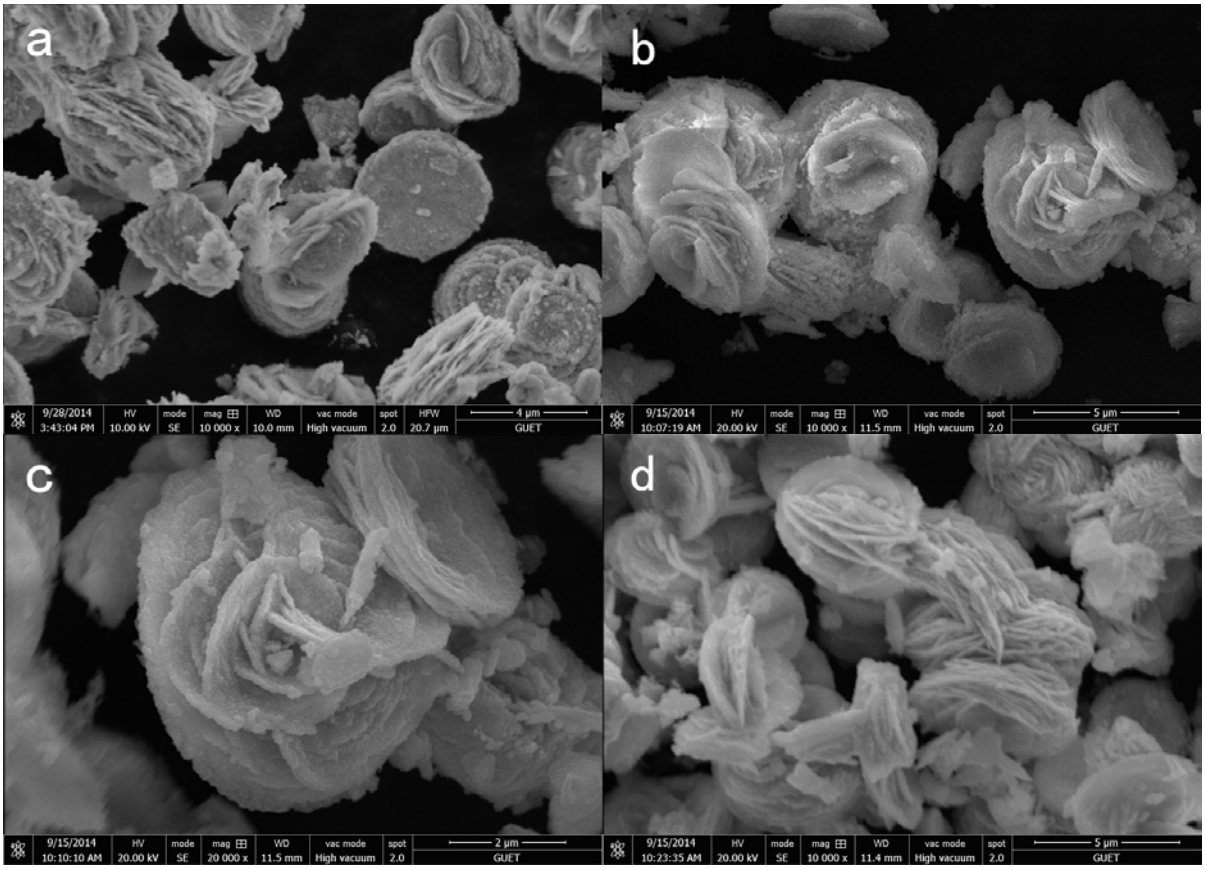

Figure 4. SEM images of pure $Bi_2Sn_2O_7$ and M-$Bi_2Sn_2O_7$: (a) $Bi_2Sn_2O_7$, (b-c) Cu-$Bi_2Sn_2O_7$, (d) Co-$Bi_2Sn_2O_7$

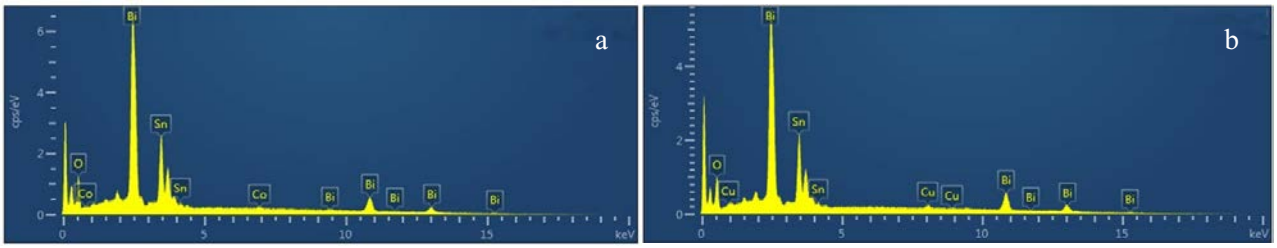

Figure 5. EDS analysis of M-$Bi_2Sn_2O_7$ powders: (a) Co-$Bi_2Sn_2O_7$, (b) Cu-$Bi_2Sn_2O_7$

3.2. UV-visible absorption spectra

The optical absorption properties of semiconductor materials are essential to determine their photocatalytic activities. Diffuse reflection spectra of the pure $Bi_2Sn_2O_7$ and M-$Bi_2Sn_2O_7$ catalysts are shown in Figure 6(a). It can be found that all of the samples show very good absorption in the visible region. An obvious red shift in spectra can be observed for the Cu- and Co-doped $Bi_2Sn_2O_7$ compared to that of pure $Bi_2Sn_2O_7$. The considerable absorption band in the visible light region would make full use of sunlight for the degradation of the pollutants. For a crystalline semiconductor, the band gap energy (E_g, in eV) of catalyst can be calculated according to the following equation [21]:

$$(\alpha h\nu)^n = A\,(h\nu - E_g)$$

Where α, $h\nu$, E_g and A are an absorption coefficient, the absorption energy, band gap, and a constant, respectively. Here n depends on the characteristic of the transition in a crystalline semiconductor [22].

For $Bi_2Sn_2O_7$, the value of *n* is 1/2 for the indirect transition [23]. The E_g of $Bi_2Sn_2O_7$ can be estimated from a plot of $(\alpha hv)^2$ versus the photon energy *hv*. The intercept of the tangent to the *x* axis gives rise to a good approximation of the E_g value for as-prepared $Bi_2Sn_2O_7$ photocatalysts. As depicted in Figure 6(b), the band gap of pure $Bi_2Sn_2O_7$ is about 2.75 eV, which is similar to the previously reported values [24]. The band gap of Cu-$Bi_2Sn_2O_7$ is 2.72 eV and that of Co-doped $Bi_2Sn_2O_7$ is about 2.68 eV. The measured results have suggested the photocatalytic activity of metal loaded catalysts would be better than that of pure $Bi_2Sn_2O_7$ catalyst with response to visible light irradiation.

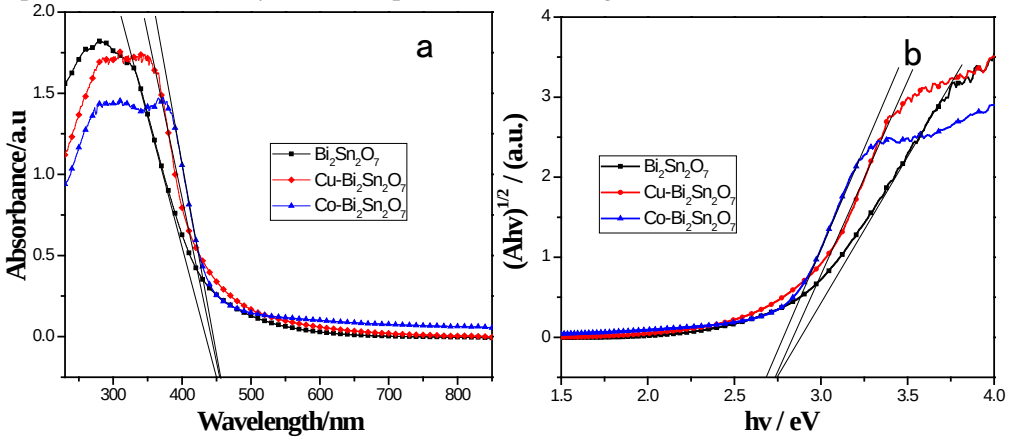

Figure 6. (a) UV-vis diffuse absorption spectra and (b) estimated band gap of pure $Bi_2Sn_2O_7$ and M-$Bi_2Sn_2O_7$ photocatalysts.

3.3. PL emission spectra

In order to establish the above analysis, the photoluminescence (PL) spectra of pure $Bi_2Sn_2O_7$ and M-$Bi_2Sn_2O_7$ photocatalysts were further measured because it can disclose the migration, transfer, and recombination processes of the photo-generated electron-hole pairs. As shown in Figure 7, an obvious peak at 520 nm in the PL spectrum for pure $Bi_2Sn_2O_7$ can be found, which is attributed to the recombination of holes and electrons in the valence band and conduction band. Apparently, the M-$Bi_2Sn_2O_7$ composite exhibits a much lower emission intensity than pure $Bi_2Sn_2O_7$, implying that the recombination of photo-generated electrons and holes is inhibited.

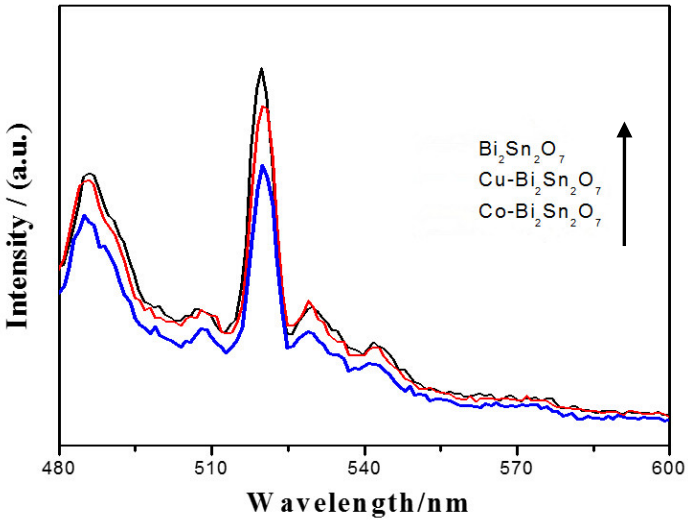

Figure 7. PL spectra of pure $Bi_2Sn_2O_7$ and metal-loaded $Bi_2Sn_2O_7$ samples

3.4. Photocatalytic activity

The photocatalytic performance of all the samples were studied by the decomposition of RhB under visible-light irradiation and presented in Figure 8, where C and C_0 represent the time-dependent concentration and the initial concentration of pollutants solution, respectively. As shown in Figure 8, the degradation efficiency of RhB of pure $Bi_2Sn_2O_7$ is about 59.2% after 250 min under visible-light irradiation. However, the degradation efficiency of metal-loaded $Bi_2Sn_2O_7$ catalysts shows a significant improvement compared to pure $Bi_2Sn_2O_7$. It is obvious that the about 83.6% RhB can be degraded by Cu-doped $Bi_2Sn_2O_7$ catalyst and the Co-$Bi_2Sn_2O_7$ catalyst shows the best performance of 89.5% degradation efficiency within the same period. The enhancement in photocatalytic activity of M-$Bi_2Sn_2O_7$ is probably ascribed to the generation of more active electrons and holes and the improvement of the separation of the photogenerated electron-hole pairs on the $Bi_2Sn_2O_7$ surface due to the introduction of metal particles.

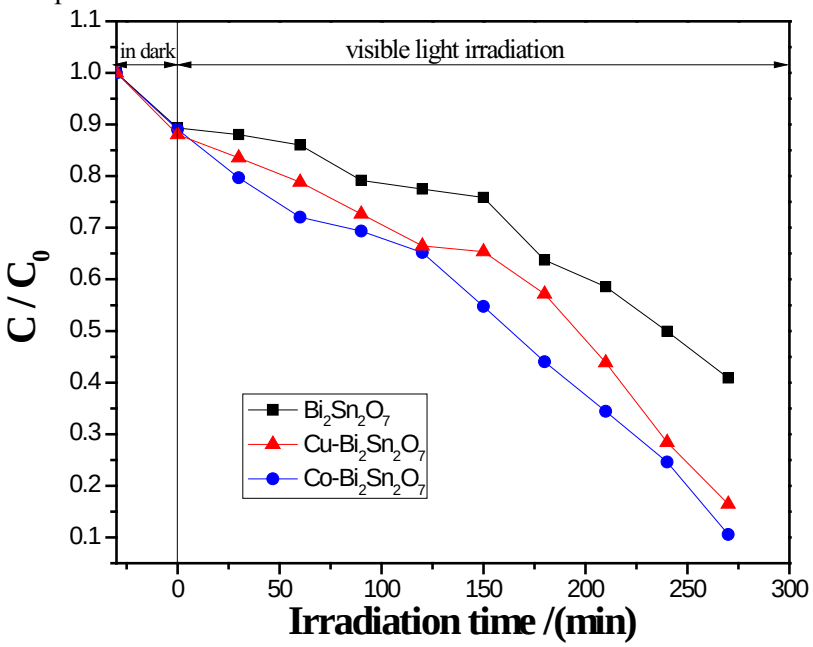

Figure 8. Photodegradation of RhB with pure $Bi_2Sn_2O_7$ and metal-loaded $Bi_2Sn_2O_7$ powders under visible-light irradiation

4. Conclusion

In summary, M-$Bi_2Sn_2O_7$ (M = Cu, Co) catalysts have been successfully synthesized by using the hydrothermal process and impregnation method. All of the as-prepared samples have been characterized by XRD, FESEM, UV-vis, IR, and PL. The degradation experiments have revealed that M-$Bi_2Sn_2O_7$ (M = Cu, Co) catalysts exhibit significant photocatalytic activity and the photocatalytic efficiency in degradation of RhB of Cu-$Bi_2Sn_2O_7$ and Co-$Bi_2Sn_2O_7$ is about 1.41 and 1.51 times compared to the pure $Bi_2Sn_2O_7$. The enhancement in photocatalytic efficiency for M-$Bi_2Sn_2O_7$ (M = Cu, Co) catalysts mainly result from the lower band-gap energies and weak fluorescence effect, which can response in visible light and lead to the more effective charge separation.

Acknowledgement

This research was supported by the National Basic Research Program of China (Grant No. 2014CB643703), the National Natural Science Foundation of China (Grant No. 11464008 and No. 51401060), the Guangxi Natural Science Foundation (Grant No. 2014GXNSFGA118001), Guangxi Key Laboratory of Information Materials (Grant No. 1210908-215-Z), and the Innovation Project of Guilin Graduate Education (Grant No. 2016YJCX20).

References

[1] Kudo A, Omori K and Kato H 1999 *J. Am. Chem. Soc.* **121** 11459
[2] Liu Z, Bai H and Sun D 2011 *Appl. Catal. B: Environ.* **104** 234
[3] Chaiwichian S, Inceesungvorn B, Wetchakun K, Phanichphant S, Kangwansupamonkon W and Wetchakun N 2014 *Mater. Res. Bull.* **54** 28
[4] Li Z, Chen X and Xue Z 2013 *J. Colloid Interface Sci.* **394** 69
[5] Chai S Y, Kim Y J and Jung M H 2009 *J. Catal.* **262** 144
[6] Xing Y, Que W and Liu X 2014 *RSC Adv.* **4** 49900
[7] Anpo M and Takeuchi M 2003 *J. Catal.* **216** 505
[8] Kikugawa N, Yang L Q, Matsumoto T and Ye J H 2010 *J. Mater. Res.* **25** 177
[9] Zhang H, Wang W, Shang M and Yin W 2010 *Catal. Commun.* **11** 982
[10] Kim H W, Shim S H, Lee J W, Park J Y and Kim S S 2008 *Chem. Phys. Lett.* **456** 193
[11] Udod L V, Sitnikov M N, Aplesnin S S and Molokeev M S 2013 *Solid State Phenomena* **215** 503
[12] Bala I, Barbar S K and Roy M 2012 *Physica B* **407** 3939
[13] Tian Q, Zhuang J and Wang J 2012 *Appl. Catal. A: Gen.* **425-426** 74
[14] Wu J J, Huang F Q, Lu X G and Chen P 2011 *J. Mater. Chem.* **21** 3872
[15] Liu H, Jin Z, Su Y and Wang Y 2015 *Sep. Purif. Technol.* **142** 25
[16] Mohameda M M and Ahmed S A 2015 *Microporous Mesoporous Mater.* **204** 62
[17] Holzwarth U and Gibson N 2011 *Nature Nanotechnology* **6** 534
[18] Long M C, Cai W M, Cai J, Zhou B X, Chai X Y and Wu Y H 2006 *J. Phys. Chem. B* **110** 20211
[19] Sun W T, Xie M Z, Jing L Q, Luan Y B and Fu H G 2011 *J. Solid State Chem.* **184** 3050
[20] Xu W C, Liu Z and Fang J Z 2013 *Int. J. Photoenergy* **2013** 394079
[21] Bian Z, Zhu Y and Zhang J 2014 *Chemosphere* **117** 527
[22] Yu K, Yang S, He H and Sun C 2009 *J. Phys. Chem. A* **113** 10024
[23] Gao E P and Wang W Z 2015 *J. Inorg. Mater.* **30** 87
[24] Xu W, Fang J and Chen Y 2015 *Mater. Chem. Phys.* **154** 30